STRUCTURAL BIOLOGY COMMUNICATIONS

ISSN 2053-230X

Crystal structure of human V-1 in the apo form

Shuichi Takeda,[a]* Ryotaro Koike,[b] Takayuki Nagae,[c] Ikuko Fujiwara,[d] Akihiro Narita,[a] Yuichiro Maéda[b] and Motonori Ota[b]

[a]Graduate School of Science, Nagoya University, Furo-cho, Chikusa-ku, Nagoya 464-8601, Japan, [b]Graduate School of Informatics, Nagoya University, Furo-cho, Chikusa-ku, Nagoya 464-8601, Japan, [c]Synchrotron Radiation Research Center, Nagoya University, Furo-cho, Chikusa-ku, Nagoya 464-8601, Japan, and [d]Graduate School of Science, Osaka City University, 3-3-138 Sugimoto, Sumiyoshi-ku, Osaka 558-8585, Japan. *Correspondence e-mail: takeda.shuichi@f.mbox.nagoya-u.ac.jp

Received 17 November 2020
Accepted 31 December 2020

Edited by I. Tanaka, Hokkaido University, Japan

Keywords: V-1; myotrophin; actin capping protein; crystal structure; *All Atom Motion Tree*; ankyrin-repeat proteins.

PDB reference: human V-1, apo form, 7df7

Supporting information: this article has supporting information at journals.iucr.org/f

V-1, also known as myotrophin, is a 13 kDa ankyrin-repeat protein that binds and inhibits the heterodimeric actin capping protein (CP), which is a key regulator of cytoskeletal actin dynamics. The crystal structure of V-1 in complex with CP revealed that V-1 recognizes CP via residues spanning several ankyrin repeats. Here, the crystal structure of human V-1 is reported in the absence of the specific ligand at 2.3 Å resolution. In the asymmetric unit, the crystal contains two V-1 monomers that exhibit nearly identical structures (C^{α} r.m.s.d. of 0.47 Å). The overall structures of the two apo V-1 chains are also highly similar to that of CP-bound V-1 (C^{α} r.m.s.d.s of <0.50 Å), indicating that CP does not induce a large conformational change in V-1. Detailed structural comparisons using the computational program *All Atom Motion Tree* revealed that CP binding can be accomplished by minor side-chain rearrangements of several residues. These findings are consistent with the known biological role of V-1, in which it globally inhibits CP in the cytoplasm.

1. Introduction

Monomeric actin polymerizes into a double-stranded filament with distinct polarity. At the leading edge of motile cells, actin filaments elongate as they direct the fast-growing barbed end towards the plasma membrane, thereby providing the driving force for migration (Fujiwara *et al.*, 2018). The heterodimeric actin capping protein (CP) is a key regulator of barbed end dynamics (Edwards *et al.*, 2014) because it can block polymerization and depolymerization at this end (Isenberg *et al.*, 1980; Schafer *et al.*, 1996; Kuhn & Pollard, 2007). Crystal structures of CP revealed that the two CP subunits, namely α and β, are associated closely and resemble a mushroom (Yamashita *et al.*, 2003; Eckert *et al.*, 2012). The C-terminal regions of each subunit located on the top of the mushroom crown, called the tentacles, are responsible for barbed-end capping (Yamashita *et al.*, 2003; Wear *et al.*, 2003). A cryo-EM study suggested that CP caps the barbed end in a two-step process: initial binding of the α-tentacle to the boundary of the two barbed-end actin subunits followed by the supportive binding of the β-tentacle to the terminal actin subunit (Narita *et al.*, 2006).

V-1, also known as myotrophin, is a 13 kDa CP inhibitor that is conserved from amoeba to mammals. V-1 has been implicated in a variety of cellular processes, such as neural development (Taoka *et al.*, 1994), endocrine function (Yamakuni *et al.*, 1998), cardiac hypertrophy (Gupta *et al.*, 2002) and insulin secretion (Poy *et al.*, 2004). V-1 is an ankyrin-repeat

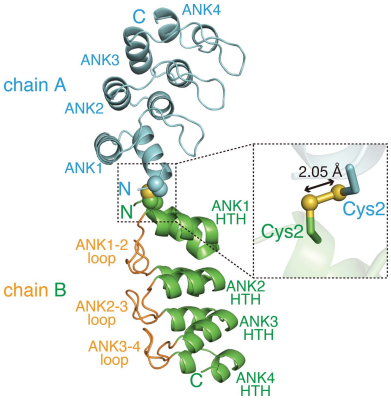

protein. A typical single ankyrin repeat consists of 30–34 amino acids that contain a helix–turn–helix motif in the middle. The core helix–turn–helix motifs are stacked tandemly and are connected by long loops (Li *et al.*, 2006). A solution NMR analysis (Yang *et al.*, 1998) revealed that V-1 comprises four ankyrin repeats: two full repeats are sandwiched by imperfect N- and C-capping repeats (we refer to these repeats as ANK1 to ANK4 from the N-terminus to the C-terminus). Domains consisting of ankyrin repeats are usually involved in protein–protein interactions. CP is the only binding partner confirmed to date for V-1 (Taoka *et al.*, 2003; Bhattacharya *et al.*, 2006). X-ray (Takeda *et al.*, 2010) and NMR (Zwolak, Fujiwara *et al.*, 2010) studies demonstrated that V-1 binds directly to the primary actin-binding site of CP, the α-tentacle, thereby sequestering CP in an inactive CP–V-1 complex that cannot cap the barbed end. The binding of V-1 to CP is regulated by other CP-binding proteins, such as CARMIL, a multidomain protein that binds CP away from the α-tentacle through an intrinsically disordered region and allosterically dissociates V-1 from CP (Yang *et al.*, 2005; Fujiwara *et al.*, 2010; Takeda *et al.*, 2010, 2011; Zwolak, Uruno *et al.*, 2010).

A series of thoughtful studies have established that the ability of V-1 to inactivate CP is pivotal for regulating the formation of actin networks *in vitro* (Fujiwara *et al.*, 2014) and *in vivo* (Jung *et al.*, 2016). It is thus of great importance to understand the mechanism of CP recognition by V-1. Although crystal structures of free CP (Yamashita *et al.*, 2003; Takeda *et al.*, 2010) and the CP–V-1 complex (Takeda *et al.*, 2010) have been reported, the structure of free V-1 has only been analyzed by solution NMR (Yang *et al.*, 1998), which revealed the basic fold of the protein, thus making important contributions to the field. However, judging from the validation scores provided by the PDB server (PDB entry 1myo; clashscore 81, Ramachandran outliers 17.1%; Yang *et al.*, 1998), the NMR structure may not be appropriate for detailed structural analyses. Here, we report the crystal structure of human V-1 in the apo form at 2.3 Å resolution with high quality (clashscore 2, Ramachandran outliers 0%). The structure of apo V-1 is strikingly similar to that of CP-bound V-1 down to the side-chain conformations. Our results demonstrated that V-1 is a constitutively active CP inhibitor that readily binds CP with minimal structural optimization.

2. Materials and methods

2.1. Macromolecule production

A brief description of the purification method for human V-1 (UniProt entry P58546) has previously been provided (Takeda *et al.*, 2010). Here, we describe the expression and purification methods of human V-1 in detail. Forward and reverse oligonucleotide primers (Table 1) were used to amplify the human full-length V-1 cDNA (residues 1–118) from the pCMV-SPORT6 vector carrying V-1 cDNA (Mammalian Gene Collection clone ID 3876632). The amplified cDNA fragment was ligated into the pGEX-6P-1 expression vector (GE Healthcare) linearized with BamHI and EcoRI. The expression vector encodes an N-terminal glutathione *S*-transferase (GST) tag followed by a human rhinovirus (HRV) 3C protease cleavage site ahead of the N-terminus of V-1.

Table 1
Macromolecule-production information.

Source organism	*Homo sapiens*
DNA source	Mammalian Gene Collection clone ID 3876632
Forward primer†	5′-CGCGGATCCATGTGCGACAAGGAGTTCATG-3′
Reverse primer‡	5′-CCGGAATTCTCACTGGAGAAGAGCTTTGATTGC-3′
Cloning vector	pGEX-6P-1
Expression vector	pGEX-6P-1
Expression host	*E. coli* BL21 (DE3)
Complete amino-acid sequence of the construct produced§	*MSPILGYWKIKGLVQPTRLLLEYLEEKYEE HLYERDEGDKWRNKKFELGLEFPNLPYY IDGDVKLTQSMAIIRYIADKHNMLGGCP KERAEISMLEGAVLDIRYGVSRIAYSKD FETLKVDFLSKLPEMLKMFEDRLCHKTY LNGDHVTHPDFMLYDALDVVLYMDPMCL DAFPKLVCFKKRIEAIPQIDKYLKSSKY IAWPLQGWQATFGGGDHPPKSDLEVLFQ* **GPLGS**MCDKEFMWALKNGDLDEVKDYVA KGEDVNRTLEGGRKPLHYAADCGQLEIL EFLLLKGADINAPDKHHITPLLSAVYEG HVSCVKLLLSKGADKTVKGPDGLTAFEA TDNQAIKALLQ

† The BamHI site is underlined. ‡ The EcoRI site is underlined. § The GST-tag sequence is in italics, the human V-1 sequence is underlined and the HRV 3C protease cleavage site is in bold.

The pGEX-6P-1-V-1 expression vector was used to transform *Escherichia coli* BL21 (DE3) cells (Thermo Fisher). The transformed cells were grown in LB broth at 310 K in the presence of 100 µg ml^{-1} ampicillin to an optical density of 1.2 at 600 nm and protein expression was induced by the addition of 0.1 m*M* isopropyl β-D-1-thiogalactopyranoside at 289 K. After 16 h of induction, the cells were harvested by centrifugation at 4000*g* for 10 min at 277 K. The cell pellet was resuspended in phosphate-buffered saline (PBS; 0.137 *M* NaCl, 8.1 m*M* Na_2HPO_4, 2.68 m*M* KCl, 1.47 m*M* KH_2PO_4 pH 7.4) supplemented with 1 m*M* dithiothreitol (DTT) and lysed by sonication on ice. The cell debris and membranes were pelleted by centrifugation at 20 000*g* for 30 min at 277 K. The soluble N-terminally GST-tagged V-1 was applied onto glutathione resin (Glutathione Sepharose 4B; GE Healthcare). To remove the GST tag, the protein-bound resin was incubated with HRV 3C protease (100 units ml^{-1}) for 16 h at 277 K. Tag-cleaved V-1 was obtained as the flowthrough and was purified by anion-exchange column chromatography (HiTrap Q; GE Healthcare) using a linear KCl gradient from 0.05 to 1 *M* in a buffer consisting of 20 m*M* Tris–HCl pH 8.0, 1 m*M* DTT. The pooled V-1 fractions were dialyzed at 277 K against a buffer consisting of 5 m*M* Tris–HCl pH 8.0, 1 m*M* DTT and were concentrated to 6 mg ml^{-1} using a Vivaspin centrifugal concentrator (molecular-weight cutoff 3000; Sartorius). The protein concentration was estimated from the absorbance at 280 nm using an extinction coefficient of 9970 M^{-1} cm^{-1} per monomer. Macromolecule-production information is summarized in Table 1.

Table 2
Crystallization.

Method	Sitting-drop vapor diffusion
Plate type	96-well crystallization plate; VCP-1 (Violamo)
Temperature (K)	293
Protein concentration (mg ml^{-1})	6
Buffer composition of protein solution	5 m*M* Tris–HCl pH 8.0, 1 m*M* DTT
Composition of reservoir solution	0.2 m*M* ammonium acetate, 20% PEG 3350
Volume and ratio of drop	0.6 µl, 1:1 ratio of protein:reservoir solution
Volume of reservoir (µl)	50

2.2. Crystallization

Crystals of human V-1 were obtained using the sitting-drop vapor-diffusion method. Equal amounts (0.3 µl) of concentrated V-1 and reservoir solution (0.2 m*M* ammonium acetate, 20% PEG 3350) were mixed on a sitting-drop plate (VCP-1; Violamo). The drop initially contained 0.5 m*M* DTT as the reducing agent carried over from the protein eluent. Cubic crystals (20 × 20 × 10 µm) grew after one month of incubation at 293 K. Crystallization information is summarized in Table 2.

2.3. Data collection and processing

The crystals were cryoprotected by transferring them into reservoir solution supplemented with 10% ethylene glycol and were flash-cooled in liquid nitrogen. X-ray diffraction data were collected on SPring-8 beamline BL41XU (Hasegawa *et al.*, 2013) using the helical data-collection method with the aid of the *KAMO* software (Yamashita *et al.*, 2018). Diffraction data from two crystals were processed and merged with *XDS* (Kabsch, 2010). Data-collection and processing statistics are summarized in Table 3.

2.4. Structure solution and refinement

The structure of apo V-1 was determined by molecular replacement with *MOLREP* (Vagin & Teplyakov, 2010) using the V-1 structure excised from the crystal structure of the CP–V-1 complex (PDB entry 3aaa; Takeda *et al.*, 2010) as a search model. Model building and refinement were performed with *Coot* (Emsley *et al.*, 2010) and *phenix.refine* (Afonine *et al.*, 2012). The final model contains two V-1 monomers in the asymmetric unit. Chain *A* comprises V-1 residues 1–117. Chain *B* comprises V-1 residues 1–117, which were N-terminally flanked by Gly-Ser derived from the HRV 3C protease cleavage site. The structure was validated using *MolProbity* (Chen *et al.*, 2010) within the *Phenix* suite (Liebschner *et al.*, 2019). Refinement statistics are summarized in Table 4. All structural figures were prepared using *PyMOL* (http://www.pymol.org/2/). Atomic coordinates and structure factors have been deposited in the Protein Data Bank (PDB entry 7df7).

2.5. Size-exclusion column chromatography

The oligomeric state of V-1 under cytosolic conditions was analyzed by size-exclusion column chromatography. Human V-1 was loaded onto a Superdex 200 10/300 column (GE Healthcare) equilibrated with PBS supplemented with 1 m*M* DTT and run at a flow rate of 0.5 ml min^{-1} at 277 K. Protein elution was monitored using the absorbance at 280 nm. Ribonuclease A (molecular weight 13 700), carbonic anhydrase (molecular weight 29 000) and ovalbumin (molecular weight 43 000) were used to calibrate the column.

Table 3
Data collection and processing.

Diffraction source	BL41XU, SPring-8
Wavelength (Å)	1.0000
Temperature (K)	100
Detector	PILATUS3 6M
Crystal-to-detector distance (mm)	250
Rotation range per image (°)	0.1
Total rotation range (°)	180
Exposure time per image (s)	0.1
Space group	$P2_12_12_1$
a, *b*, *c* (Å)	49.62, 56.28, 81.10
α, β, γ (°)	90, 90, 90
Mosaicity (°)	0.1
Resolution range (Å)	46.31–2.30 (2.36–2.30)
Total No. of reflections	135479 (8910)
No. of unique reflections	10568 (757)
Completeness (%)	99.8 (97.4)
Multiplicity	12.8 (11.8)
$\langle I/\sigma(I)\rangle$	21.8 (2.1)
$R_{\rm r.i.m.}$	0.074 (1.284)
Overall *B* factor from Wilson plot (Å^2)	61.55

Table 4
Structure solution and refinement.

Resolution range (Å)	46.24–2.30 (2.53–2.30)
Completeness (%)	99.8 (99.2)
σ Cutoff	$F > 1.35\sigma(F)$
No. of reflections, working set	10038 (2438)
No. of reflections, test set	529 (128)
Final $R_{\rm cryst}$	0.218 (0.269)
Final $R_{\rm free}$	0.248 (0.327)
Cruickshank DPI	0.376
No. of non-H atoms	
Total	1828
Protein	1799
Ligand	0
Water	29
R.m.s. deviations	
Bonds (Å)	0.003
Angles (°)	0.513
Average *B* factors (Å^2)	
Protein	60.6
Ramachandran plot	
Most favored (%)	98.7
Allowed (%)	1.3

2.6. *All Atom Motion Tree* (*AAMT*)

Motion Tree (*MT*) creates a diagram that describes structural changes between two structures of an identical protein based on C$^\alpha$ atoms (Koike *et al.*, 2014). *All Atom Motion Tree* (*AAMT*) is an enhanced version of *MT* for detecting structural changes, including those of side chains, based on the coordinates of all heavy atoms (Koike & Ota, 2019). Firstly, the protein structure is represented by a distance matrix, in which the distances of pairs of heavy atoms are calculated as matrix elements. Next, the difference matrix of two distance matrices is calculated. Finally, a hierarchical clustering method

is applied to the distance difference matrix to obtain a tree diagram called the All Atom Motion Tree (AAMT).

AAMT identifies rigid bodies in the protein at any magnitude of motion and presents them in a hierarchical manner. At the first node from the root, the whole protein is divided into two rigid bodies and the relative motion of the two rigid bodies describes the largest structural change between the two protein structures. Each rigid body is further divided into two smaller rigid bodies at the descendant nodes. Effective nodes were introduced to indicate significant rigid-body motions, where a rigid body consisting of more than ten atoms is divided into two rigid bodies each containing at least three atoms. The magnitude of an effective node is more than 4.5 Å. Only rigid bodies at the effective nodes were considered.

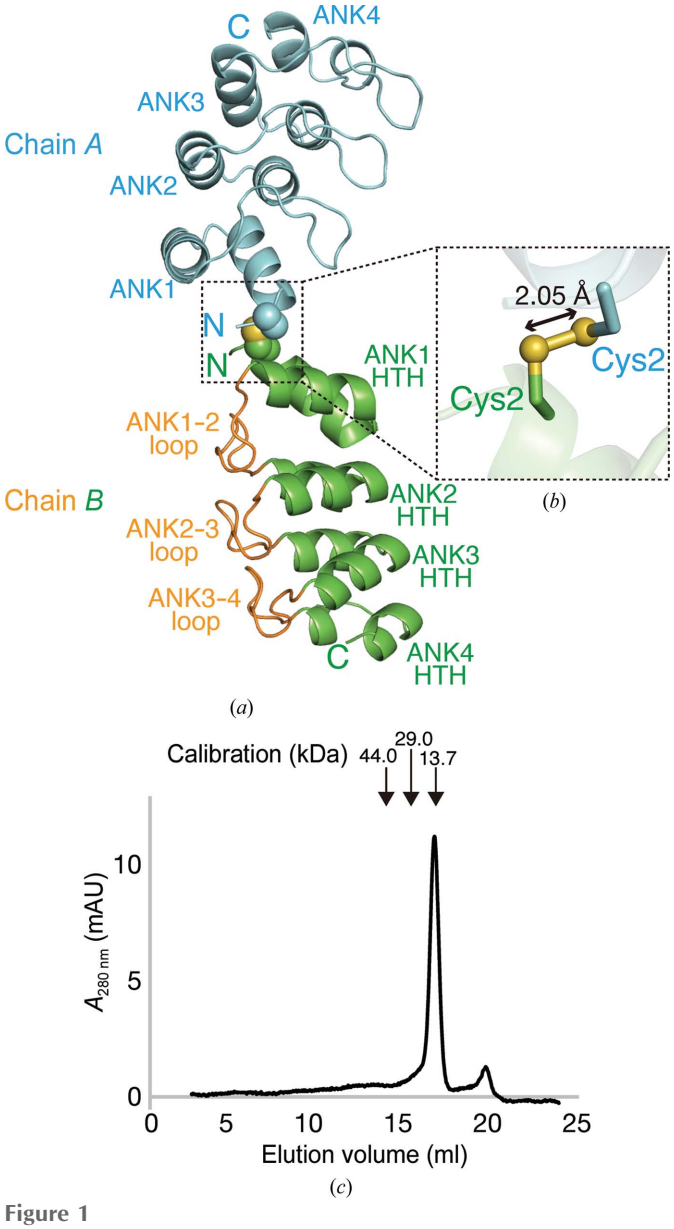

Figure 1
Crystal structure of human V-1 in the apo form. (*a*) Overall structure of human V-1 in the asymmetric unit. The whole of chain *A* is shown in cyan. Helix–turn–helix regions and loop regions of chain *B* are shown in green and orange, respectively. The N- and C-termini of each chain are indicated. Cys2 residues are shown as spheres. (*b*) Close-up view of the S—S bond formed at the noncrystallographic dimer interface. (*c*) Size-exclusion column chromatography. Human V-1 was run through a Superdex 200 10/300 size-exclusion column equilibrated with PBS supplemented with 1 m*M* DTT. Protein elution was monitored by the absorbance at 280 nm. The elution positions of size markers, namely ribonuclease A (molecular weight 13 700), carbonic anhydrase (molecular weight 29 000) and ovalbumin (molecular weight 43 000), are indicated by arrows.

3. Results and discussion

3.1. Overall structure of apo human V-1

Human V-1 was crystallized in the absence of ligand molecules and its structure was determined at 2.3 Å resolution (Fig. 1*a*). The overall *MolProbity* score is 0.92, indicating that the model quality is sufficient for detailed structural analysis. The asymmetric unit contains two V-1 monomers, namely chains *A* and *B*, that share almost identical main-chain structures (C^{α} r.m.s.d. of 0.47 Å). The two chains contact each other via the N-terminal ANK1 helix of each monomer (Fig. 1*a*). In the interface, two S atoms, from Cys2 of chains *A* and *B*, are located at a distance of 2.05 Å, indicating that a disulfide bond is formed within the crystal (Fig. 1*b*). It is unlikely that disulfide-bond-mediated homodimerization is a biological assembly because V-1 resides in the cytoplasm, which has a reducing environment (Nishikawa & Ooi, 1982). We performed size-exclusion column chromatography and found that the purified V-1 used for crystallization eluted as a single peak with an elution volume corresponding to the molecular weight of a monomer (13 306) in an eluent composed of PBS supplemented with a reducing agent (1 m*M* DTT; Fig. 1*c*). V-1 was observed as a monomer in a solution NMR study (Yang *et al.*, 1998). We assumed that the reducing agent that was initially contained in the crystallization drop (0.5 m*M* DTT) had become less effective during incubation (approximately one month), allowing the formation of the disulfide bond at the noncrystallographic dimer interface. Notably, the N-terminus of rat V-1 is post-translationally modified *in vivo*: Met1 was cleaved co-translationally and Cys2 was *N*-acetylated (Taoka *et al.*, 1992). This differs from the *E. coli*-expressed V-1 protein we used for crystallization. Recombinant V-1 retains Met1, which is flanked by two residues derived from the HRV 3C protease cleavage site: Gly (−1) and Ser (0).

3.2. Comparisons of the main-chain structures between apo and CP-bound V-1

The backbone structures of the two apo V-1 chains are highly similar to that of V-1 in complex with CP (C^{α} r.m.s.d.s of 0.36 and 0.40 Å for chains *A* and *B*, respectively; Figs. 2*a* and 2*b*), demonstrating that CP binding does not induce a large conformational change in V-1. The three V-1 chains, namely chains *A* and *B* in the apo form and the CP-bound form, exhibit almost identical main-chain traces in the helix–turn–helix regions [C^{α} r.m.s.d.s of <0.50 Å; residues 1–24 (ANK1), 38–57 (ANK2), 71–90 (ANK3) and 104–118 (ANK4); Figs. 2*a* and 2*b*], in which the four tandemly stacked repeats are

stabilized primarily by hydrophobic interactions (Yang *et al.*, 1998). Interestingly, the loop regions, namely residues 25–37 (ANK1–2), 58–70 (ANK2–3) and 91–103 (ANK3–4), which protrude outwards from the molecule, are structurally less diverse than the core helix–turn–helix regions (C^{α} r.m.s.d.s of <0.33 Å; Figs. 2*a* and 2*b*). This may be owing to a number of intra- and inter-ankyrin-repeat hydrogen bonds that stabilize the loop structures (Fig. 2*c*). The striking structural similarity among the three V-1 polypeptide chains, which are packed in different environments in the crystals, suggests that the entire molecule of V-1 adopts the same rigid conformation regardless of the presence or absence of CP. In support of this notion, CD spectra analysis showed that V-1 has a stably folded structure under a variety of solution conditions (Mosavi *et al.*, 2002).

3.3. Side-chain conformational changes detected by *All Atom Motion Tree*

We next comprehensively analyzed the conformational changes of V-1 side chains induced by CP binding using the computational program *All Atom Motion Tree* (*AAMT*; Koike & Ota, 2019). By comparing a pair of independently obtained structures of an identical protein using all heavy atoms comprising the polypeptide chains (*i.e.* including the side-chain atoms), *AAMT* detects a wide range of rigid-body motions, not only global domain motions but also local structural changes related to the side-chain motions. We used *AAMT* to compare the apo V-1 structure (chain *B*) with the CP-bound structure (Fig. 3). Similar results were obtained from the comparison using the apo chain *A* (data not shown). *AAMT* did not detect large conformational changes, confirming that the two conformations were essentially identical except for local conformational variations.

AAMT detected side-chain motions of only five V-1 residues, namely Lys4 (node #1), Tyr21 (node #2), Trp8 (node #3), Lys66 (node #4) and Gln111 (node #5), as effective nodes of the dendrogram (Figs. 3*a* and 3*b*). Lys4 (node #1) and Gln111 (node #5) are located away from the CP interface and their side chains do not contact the surrounding residues in either structure; therefore, the observed mobility seems to be owing to the flexibility of free-standing side chains.

Trp8 (node #3) is a key residue in CP binding because the replacement of this tryptophan with alanine reduced the affinity for CP 300-fold (Takeda *et al.*, 2010). Trp8 undergoes a 180° side-chain flip upon CP binding to avoid a steric clash with the V-1 binding loop of the CP β-subunit (residues

C^{α} r.m.s.d.s

	Apo chain *A*	Apo chain *B*
Apo chain *B*	0.47/0.46/0.33	
CP-bound	0.36/0.36/0.33	0.40/0.49/0.24

Overall/helix–turn–helix region/loop region (Å)

(*a*)

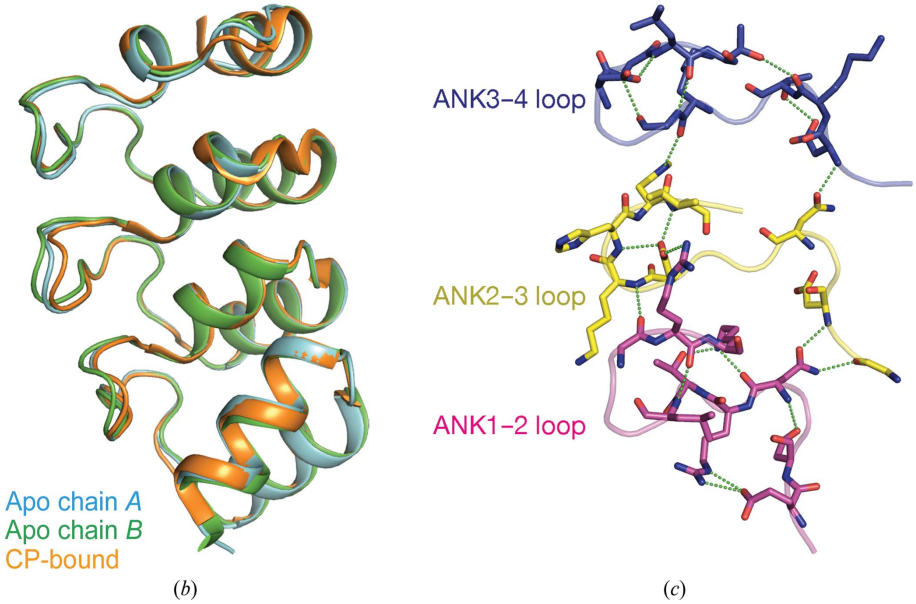

(*b*) (*c*)

Figure 2
Comparisons of main-chain structures. (*a*) C^{α} root-mean-square deviations (r.m.s.d.s) for apo V-1 (this study) and CP-bound V-1 (PDB entry 3aaa) structures. Values corresponding to the whole molecule, helix–turn–helix regions and loop regions are listed in that order. (*b*) Superposition of two apo V-1 structures (cyan and green) and CP-bound V-1 (orange). (*c*) Intra-loop and inter-loop interactions. Loop regions of the apo V-1 structure (chain *A*) are shown in different colors. Residues participating in interactions are shown as sticks. Green dotted lines indicate hydrogen bonds.

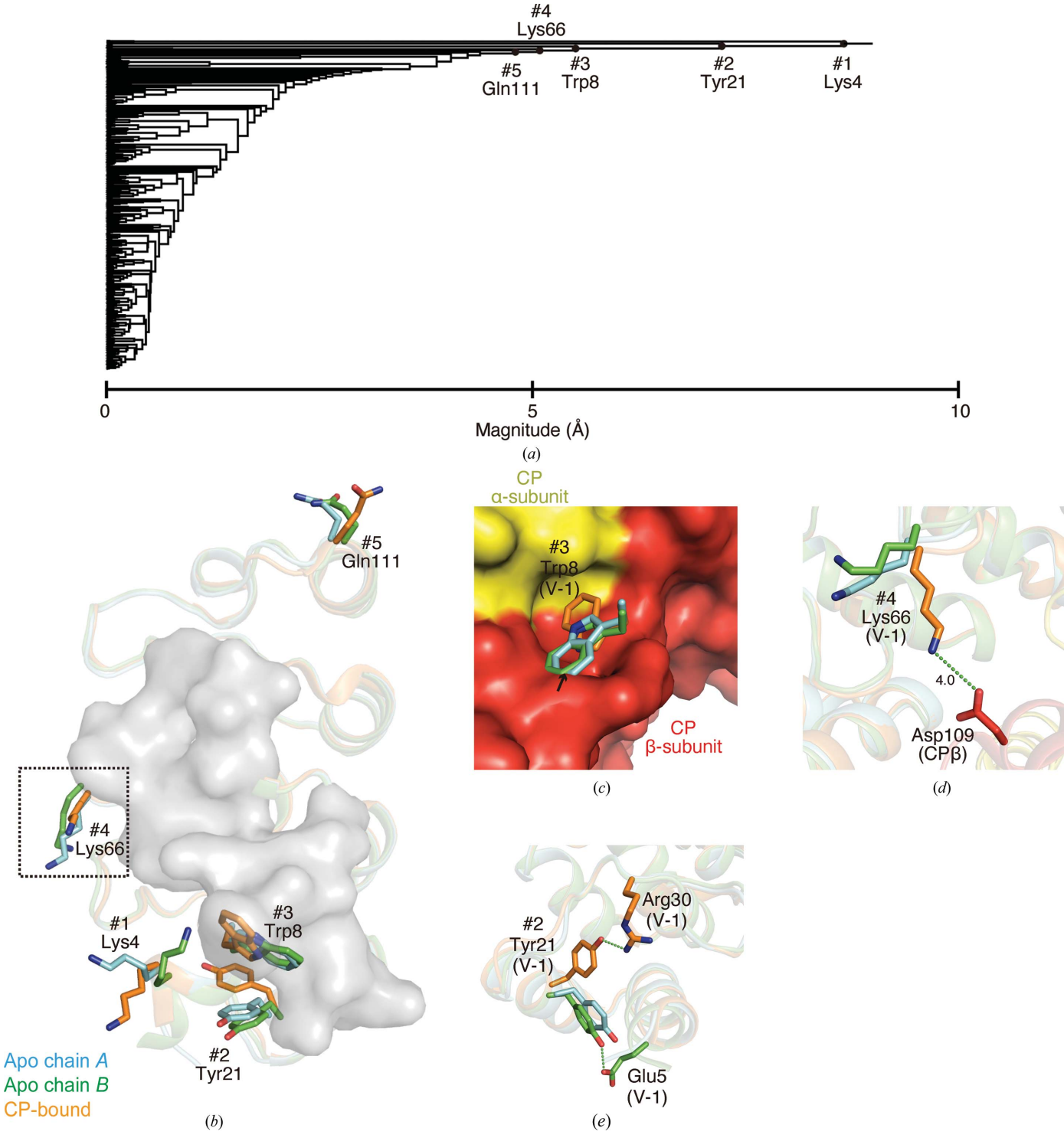

Figure 3
All Atom Motion Tree (AAMT). (*a*) AAMT between apo chain *B* and CP-bound V-1. *AAMT* detected five effective nodes (magnitudes larger than 4.5 Å; shown as black circles with numbers), all of which represent local motions of side-chain atoms (smaller rigid bodies) relative to the remaining part of the V-1 molecule (larger rigid bodies). (*b*) Positions and orientations of five residues whose structural changes were detected by *AAMT*. Lys66 is highlighted by a dotted square as in Fig. 4(*c*). The light gray surface indicates the CP binding surface. (*c*) A close-up view of Trp8 of V-1 (node #3). CP α- and β-subunits are shown as yellow and red surfaces, respectively. In the monomeric orientation (cyan and green), Trp8 clashes with CP (indicated by an arrow). The 180° rotation of the side chain allows Trp8 to fit into a pocket created between the two CP subunits (orange). (*d*) The interaction between Lys66 (V-1; node #4) and Asp109 (CP β-subunit) in the CP–V-1 complex. A possible salt bridge is indicated by a green dotted line, with the distance shown in Å. (*e*) The side-chain flip of Tyr21 (node #2) upon CP binding. Hydrogen bonds are indicated by green dotted lines. The conformational change of Tyr21 does not affect the main-chain structure of V-1.

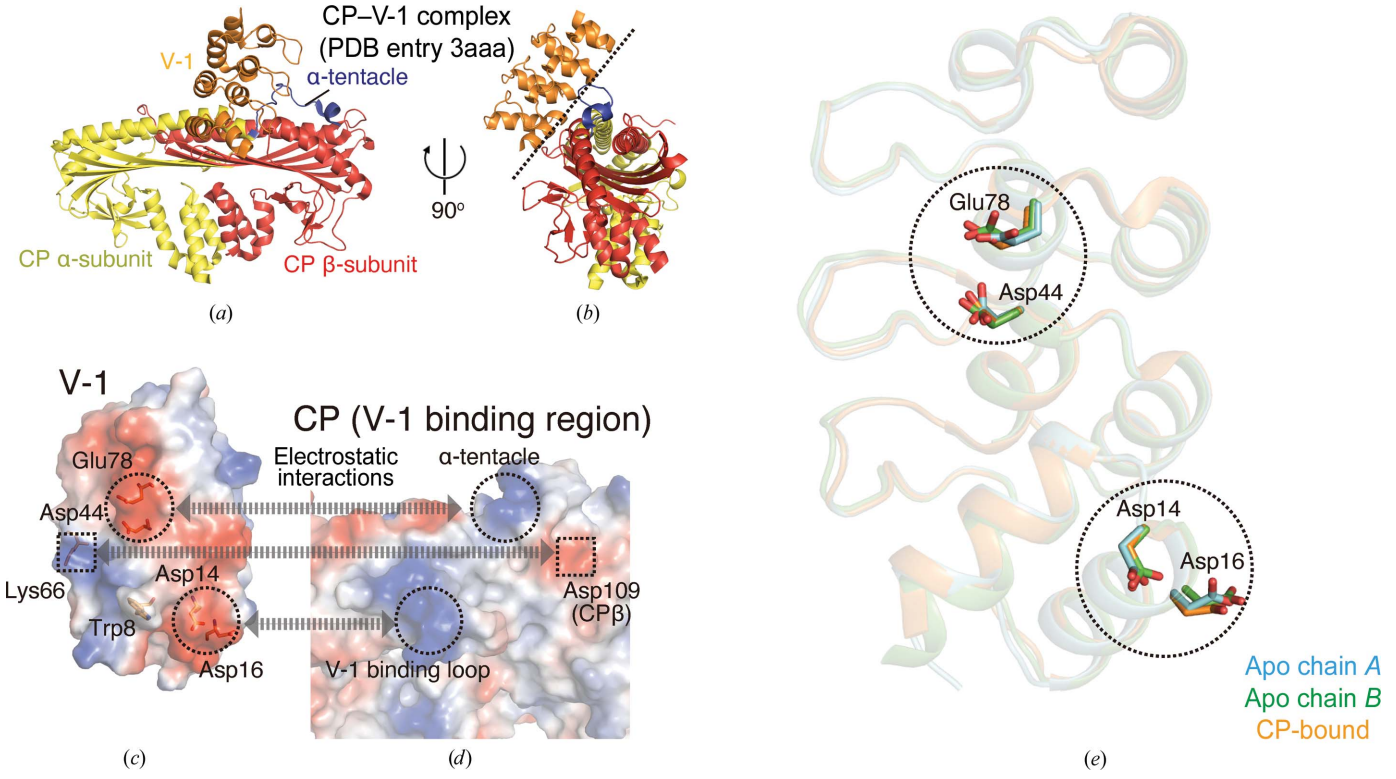

Figure 4
Structural changes detected by *AAMT*. (*a*, *b*) Overall structure of the CP–V-1 complex (PDB entry 3aaa). Two orthogonal views are shown. The CP α-subunit, β-subunit and V-1 are shown in yellow, red and orange, respectively. The CP α-tentacle is highlighted in blue. The cross-section of the molecular interface is indicated by a dotted line in (*b*). (*c*, *d*) Electrostatic surface renderings of V-1 (*c*) and the V-1 binding region of CP (*d*). Complementary acidic or basic patches on each molecule are indicated by dotted circles. Positions of Lys66 (V-1) and Asp109 (CPβ) identified by the *AAMT* analysis are indicated by dotted squares. V-1 residues involved in CP binding are shown as sticks in (*c*). Two basic patches on CP molecules are (i) the α-tentacle, which contains the basic triad residues (Lys256, Arg260 and Arg266 of CPα) important for barbed-end capping (Wear *et al.*, 2003; Narita *et al.*, 2006; Kim *et al.*, 2010), and (ii) the V-1 binding loop connecting the fifth and sixth strands of the CP β-subunit (residues 138–144 of CPβ) (Takeda *et al.*, 2010; Zwolak, Fujiwara *et al.*, 2010; Koike *et al.*, 2016). (*e*) Positions and orientations of acidic residues on the CP interface. Acidic patches are circled as in (*c*).

138–144) and to fit into the binding pocket of CP (Fig. 3*c*). The rotameric states of Trp8 in apo V-1 (chain *A*) and CP-bound V-1 are t90 (χ_1 = 174.8° and χ_2 = 91.5°) and t-105 (χ_1 = 174.4° and χ_2 = −97.9°), respectively. It is likely that Trp8 can easily adopt either rotameric state because both rotamers are major conformations of tryptophan that are observed frequently in protein structures (Lovell *et al.*, 2000).

Lys66 (node #4) is present in the ANK2–3 loop and its side chain appears to be highly mobile in apo V-1. In CP-bound V-1, Lys66 extends towards Asp109 of the CP β-subunit, with a distance between the Lys66 N^{ζ} and Asp109 $O^{\delta2}$ atoms of 4.0 Å, indicating that the two residues form an intermolecular salt bridge (Fig. 3*d*). The CP-binding residues of V-1 reported thus far are located in the helix–turn–helix regions (see below). Interaction mediated by residues in the loop region has not previously been described.

Tyr21 (node #2) is positioned near the C-terminus of the second helix in AKN1 and the side chain is not exposed on the V-1 surface. The side-chain O atom of Tyr21 forms a hydrogen bond to Glu5 on the N-terminal helix in the apo form (Fig. 3*e*). Upon CP binding, Tyr21 flips the side chain 90° and forms a new hydrogen bond to Arg30, which is located in the ANK1–2 loop (Fig. 3*e*). The swapping of the hydrogen-bonding partner does not directly affect the main-chain structure. In *Dictyostelium* V-1, Ser22, which occupies an analogous position to Tyr21 in human V-1, is phosphorylated and the phosphorylation-mimicking mutant of V-1, Ser22Glu, had an impaired CP inhibition activity (Jung *et al.*, 2016). Thus, it is possible that the residue in this position acts as a switch to regulate the affinity of V-1 for CP through a mechanism that has yet to be identified.

The formation of the CP–V-1 complex is based on electrostatic interactions (Figs. 4*a*–4*d*; Takeda *et al.*, 2010; Zwolak, Fujiwara *et al.*, 2010). Four acidic residues spanning three ankyrin repeats, namely Asp14 and Asp16 (ANK1), Asp44 (ANK2) and Glu78 (ANK3), are important for CP binding. Mutations of these residues greatly impair the affinity for CP (Takeda *et al.*, 2010). *AAMT* demonstrated that the conformations of key acidic residues are nearly identical in apo and CP-bound V-1 (Figs. 3*a* and 4*e*).

4. Conclusions

Domains consisting of ankyrin repeats are usually involved in protein–protein interactions, which are typically mediated

through the loop regions (Javadi & Itzhaki, 2013). The apparent flexibility of the loop regions is likely to contribute to ligand recognition by ankyrin repeats, particularly those that can bind to multiple partners, such as tumor suppressor p16 and the oncoprotein gankyrin (Li *et al.*, 2006). The loop-mediated ligand-recognition strategy has been used to design tailored ankyrin-repeat proteins (DARPins) that can bind specifically to a target molecule with high affinity (Plückthun, 2015). In contrast, V-1 binds CP mainly through residues in the helix–turn–helix regions. Our results indicate that V-1 binds CP only by the conformational optimization of a few residues, which appears to be energetically less costly. This structural feature of V-1, in which it always adopts the active form, is consistent with its proposed cellular role: V-1 sequesters CP from actin throughout the cytoplasm (Jung *et al.*, 2016). The high structural similarity between the apo and CP-bound forms suggests that V-1 is conformationally less flexible, which is in contrast to the CP-binding motif that is present in CARMIL and also to CP itself. The CP-binding motif of CARMIL is ∼20 amino acids in length and is intrinsically disordered (Yang *et al.*, 2005; Takeda *et al.*, 2010; Hernandez-Valladares *et al.*, 2010), and CP consists of two rigid domains that undergo a twisting conformational change relative to each other (Takeda *et al.*, 2010). These differences in structural flexibility among the three proteins/regions may account for the experimental results. Owing to its flexibility, CARMIL captures V-1-bound CP and shifts the conformation of CP towards a conformation that is unfavorable for V-1 binding, thus allosterically dissociating V-1 from CP (Yang *et al.*, 2005; Takeda *et al.*, 2010; Hernandez-Valladares *et al.*, 2010). By contrast, structural rigidity does not allow V-1 to interact with CARMIL-bound CP, and V-1 is ineffective in retrieving CARMIL from CP (Fujiwara *et al.*, 2014). Recent studies have identified that twinfilin, an ADF (actin depolymerization factor)/cofilin protein, is involved in the regulation of CP–V-1 interaction via the C-terminal tail region, which contains the CARMIL-like CP-binding motif (Johnston *et al.*, 2018; Hakala *et al.*, 2019). Our results provide insights into the mechanism by which V-1 and other CP regulators cooperatively control actin-filament dynamics in living cells.

Acknowledgements

We thank Tohru Yamakuni for critical reading of the manuscript. We thank Atsuo Suzuki for his advice on the structural analysis. The X-ray diffraction data were collected on the BL41XU beamline at SPring-8 under proposal 2017B2720. We thank Kazuya Hasegawa, Takashi Kawamura and the staff of BL41XU for their technical support during data collection.

Funding information

The following funding is acknowledged: Japan Society for the Promotion of Science (grant Nos. 16K17708 and 20K06522 to Shuichi Takeda; grant No. 17K07373 to Shuichi Takeda and Ikuko Fujiwara; and grant Nos. JP18K12217 and JP19H05390 to Ryotaro Koike).

References

Afonine, P. V., Grosse-Kunstleve, R. W., Echols, N., Headd, J. J., Moriarty, N. W., Mustyakimov, M., Terwilliger, T. C., Urzhumtsev, A., Zwart, P. H. & Adams, P. D. (2012). *Acta Cryst.* D**68**, 352–367.
Bhattacharya, N., Ghosh, S., Sept, D. & Cooper, J. A. (2006). *J. Biol. Chem.* **281**, 31021–31030.
Chen, V. B., Arendall, W. B., Headd, J. J., Keedy, D. A., Immormino, R. M., Kapral, G. J., Murray, L. W., Richardson, J. S. & Richardson, D. C. (2010). *Acta Cryst.* D**66**, 12–21.
Eckert, C., Goretzki, A., Faberova, M. & Kollmar, M. (2012). *BMC Struct. Biol.* **12**, 12.
Edwards, M., Zwolak, A., Schafer, D. A., Sept, D., Dominguez, R. & Cooper, J. A. (2014). *Nat. Rev. Mol. Cell Biol.* **15**, 677–689.
Emsley, P., Lohkamp, B., Scott, W. G. & Cowtan, K. (2010). *Acta Cryst.* D**66**, 486–501.
Fujiwara, I., Remmert, K. & Hammer, J. A. (2010). *J. Biol. Chem.* **285**, 2707–2720.
Fujiwara, I., Remmert, K., Piszczek, G. & Hammer, J. A. (2014). *Proc. Natl Acad. Sci. USA*, **111**, E1970–E1979.
Fujiwara, I., Takeda, S., Oda, T., Honda, H., Narita, A. & Maéda, Y. (2018). *Biophys. Rev.* **10**, 1513–1519.
Gupta, S., Purcell, N. H., Lin, A. & Sen, S. (2002). *J. Cell Biol.* **159**, 1019–1028.
Hakala, M., Wioland, H., Tolonen, M., Jegou, A., Romet-Lemonne, G. & Lappalainen, P. (2019). *bioRxiv*, 864769.
Hasegawa, K., Shimizu, N., Okumura, H., Mizuno, N., Baba, S., Hirata, K., Takeuchi, T., Yamazaki, H., Senba, Y., Ohashi, H., Yamamoto, M. & Kumasaka, T. (2013). *J. Synchrotron Rad.* **20**, 910–913.
Hernandez-Valladares, M., Kim, T., Kannan, B., Tung, A., Aguda, A. H., Larsson, M., Cooper, J. A. & Robinson, R. C. (2010). *Nat. Struct. Mol. Biol.* **17**, 497–503.
Isenberg, G., Aebi, U. & Pollard, T. D. (1980). *Nature*, **288**, 455–459.
Javadi, Y. & Itzhaki, L. S. (2013). *Curr. Opin. Struct. Biol.* **23**, 622–631.
Johnston, A. B., Hilton, D. M., McConnell, P., Johnson, B., Harris, M. T., Simone, A., Amarasinghe, G. K., Cooper, J. A. & Goode, B. L. (2018). *eLife*, **7**, e41313.
Jung, G., Alexander, C. J., Wu, X. S., Piszczek, G., Chen, B.-C., Betzig, E. & Hammer, J. A. (2016). *Proc. Natl Acad. Sci. USA*, **113**, E6610–E6619.
Kabsch, W. (2010). *Acta Cryst.* D**66**, 125–132.
Kim, T., Cooper, J. A. & Sept, D. (2010). *J. Mol. Biol.* **404**, 794–802.
Koike, R. & Ota, M. (2019). *Biophys. Physicobiol.* **16**, 280–286.
Koike, R., Ota, M. & Kidera, A. (2014). *J. Mol. Biol.* **426**, 752–762.
Koike, R., Takeda, S., Maéda, Y. & Ota, M. (2016). *Proteins*, **84**, 948–956.
Kuhn, J. R. & Pollard, T. D. (2007). *J. Biol. Chem.* **282**, 28014–28024.
Li, J., Mahajan, A. & Tsai, M. D. (2006). *Biochemistry*, **45**, 15168–15178.
Liebschner, D., Afonine, P. V., Baker, M. L., Bunkóczi, G., Chen, V. B., Croll, T. I., Hintze, B., Hung, L.-W., Jain, S., McCoy, A. J., Moriarty, N. W., Oeffner, R. D., Poon, B. K., Prisant, M. G., Read, R. J., Richardson, J. S., Richardson, D. C., Sammito, M. D., Sobolev, O. V., Stockwell, D. H., Terwilliger, T. C., Urzhumtsev, A. G., Videau, L. L., Williams, C. J. & Adams, P. D. (2019). *Acta Cryst.* D**75**, 861–877.
Lovell, S. C., Word, J. M., Richardson, J. S. & Richardson, D. C. (2000). *Proteins*, **40**, 389–408.
Mosavi, L. K., Williams, S. & Peng Zy, Z.-Y. (2002). *J. Mol. Biol.* **320**, 165–170.
Narita, A., Takeda, S., Yamashita, A. & Maéda, Y. (2006). *EMBO J.* **25**, 5626–5633.
Nishikawa, K. & Ooi, T. (1982). *J. Biochem.* **91**, 1821–1824.
Plückthun, A. (2015). *Annu. Rev. Pharmacol. Toxicol.* **55**, 489–511.
Poy, M. N., Eliasson, L., Krutzfeldt, J., Kuwajima, S., Ma, X., Macdonald, P. E., Pfeffer, S., Tuschl, T., Rajewsky, N., Rorsman, P.

& Stoffel, M. (2004). *Nature*, **432**, 226–230.
Schafer, D. A., Jennings, P. B. & Cooper, J. A. (1996). *J. Cell Biol.* **135**, 169–179.
Takeda, S., Koike, R., Nitanai, Y., Minakata, S., Maéda, Y. & Ota, M. (2011). *Phys. Biol.* **8**, 035005.
Takeda, S., Minakata, S., Koike, R., Kawahata, I., Narita, A., Kitazawa, M., Ota, M., Yamakuni, T., Maéda, Y. & Nitanai, Y. (2010). *PLoS Biol.* **8**, e1000416.
Taoka, M., Ichimura, T., Wakamiya-Tsuruta, A., Kubota, Y., Araki, T., Obinata, T. & Isobe, T. (2003). *J. Biol. Chem.* **278**, 5864–5870.
Taoka, M., Isobe, T., Okuyama, T., Watanabe, M., Kondo, H., Yamakawa, Y., Ozawa, F., Hishinuma, F., Kubota, M., Minegishi, A., Song, S.-Y. & Yamakuni, T. (1994). *J. Biol. Chem.* **269**, 9946–9951.
Taoka, M., Yamakuni, T., Song, S.-Y., Yamakawa, Y., Seta, K., Okuyama, T. & Isobe, T. (1992). *Eur. J. Biochem.* **207**, 615–620.
Vagin, A. & Teplyakov, A. (2010). *Acta Cryst.* D**66**, 22–25.
Wear, M. A., Yamashita, A., Kim, K., Maéda, Y. & Cooper, J. A. (2003). *Curr. Biol.* **13**, 1531–1537.
Yamakuni, T., Yamamoto, T., Hoshino, M., Song, S.-Y., Yamamoto, H., Kunikata-Sumitomo, M., Minegishi, A., Kubota, M., Ito, M. & Konishi, S. (1998). *J. Biol. Chem.* **273**, 27051–27054.
Yamashita, A., Maeda, K. & Maéda, Y. (2003). *EMBO J.* **22**, 1529–1538.
Yamashita, K., Hirata, K. & Yamamoto, M. (2018). *Acta Cryst.* D**74**, 441–449.
Yang, C., Pring, M., Wear, M. A., Huang, M., Cooper, J. A., Svitkina, T. M. & Zigmond, S. H. (2005). *Dev. Cell*, **9**, 209–221.
Yang, Y., Nanduri, S., Sen, S. & Qin, J. (1998). *Structure*, **6**, 619–626.
Zwolak, A., Fujiwara, I., Hammer, J. A. & Tjandra, N. (2010). *J. Biol. Chem.* **285**, 25767–25781.
Zwolak, A., Uruno, T., Piszczek, G., Hammer, J. A. & Tjandra, N. (2010). *J. Biol. Chem.* **285**, 29014–29026.